Journal of Materials Chemistry A

COMMUNICATION

View Article Online
View Journal | View Issue





Cite this: J. Mater. Chem. A, 2017, 5, 17828

Received 24th May 2017
Accepted 2nd August 2017

DOI: 10.1039/c7ta04521b

rsc.li/materials-a

# Epitaxial growth: rapid synthesis of highly permeable and selective zeolite-T membranes†

Yiwei Luo,[a] Youjia Lv,[a] Prashant Kumar,[b] Jingjing Chu,[a] Jianhua Yang, *[a] Michael Tsapatsis,*[b] K. Andre Mkhoyan,[b] Gaohong He, [ac] Jinming Lu[a] and Yan Zhang[a]

Dense and continuous zeolite T membranes with controlled membrane thickness similar to that of the seed layer can be obtained on both macroporous $Al_2O_3$ tubes and hollow fibers with a largely shortened synthesis time through epitaxial growth of seeds and closing of voids among seeds, exhibiting a high flux of 5.9 and 9.8 kg $m^{-2}$ $h^{-1}$ with corresponding selectivity larger than 10 000 and 3870 for a 90% isopropanol/water mixture at 348 K.

Improving the energy efficiency, increasing the share of renewable energy, and cleaner and energy-efficient technologies are important for sustainable development.[1] Membrane-based separation demonstrates great power to lower energy consumption and carbon footprint by providing alternatives to many conventional techniques such as distillation, drying and evaporation. Among the membrane materials, zeolite membranes offer outstanding potential in separation of many industrial molecular mixtures due to their molecular sieving selectivity and high thermal and mechanical stability that allows them to operate under harsh conditions.[2,3] Zeolite NaA membranes have been commercialized for the dehydration of solvents and biofuels in small- to medium-scale plants.[4,5] The low acid resistance and high cost of NaA zeolite membranes limit their wider industrial application.[6]

Compared with NaA zeolite membranes, zeolite T membranes with a Si/Al ratio of 3.0–4.0 and an effective pore size of 0.36 nm × 0.51 nm possess good acid resistance while remaining hydrophilic.[7] Therefore, zeolite T membranes can be extended to organic dehydration in an acid environment with pH as low as 3, thereby promoting the implementation of zeolite membranes in industrial plants.[8,9]

Keeping in mind that high flux, high selectivity and low cost are basic requirements for the development of separation membranes towards industrial application, many strategies have been proposed to improve the zeolite membrane performance including manipulation of crystallographic orientation,[10,11] spatial distribution of Al,[12] elimination of grain boundaries,[13] use of polymer substrates,[14] reduction of the membrane thickness by using nanosheets and nano-seeds[15,16] or using high aspect-ratio seeds.[17] However, manipulating the kinetics of zeolite growth without organic additives and with short synthesis times for the fabrication of low cost, high performance membranes is largely desired.

Herein, we report a simple but highly effective strategy through epitaxial growth of the seeds solely by regulating the kinetics of zeolite nucleation and crystal growth. By this method, highly permeable and selective zeolite T membranes can be obtained in a relatively short time.

Low-cost (200 $ per $m^2$) coarse macroporous $Al_2O_3$ tubes with an average pore size of 3–4 μm were used as a support (see ESI Fig. S1a†). The large pore size of the support is favourable for high flux due to its low mass-transfer resistance. We are interested in forming a dense membrane within the seed layer by promoting epitaxial growth of the seeds at high temperature instead of renucleation and crystallization at lower temperature. A continuous, smooth and uniform seed layer is desirable for the membrane growth within the seed layer to be achieved. Such seed layers, as shown in Fig. 1a and b, were synthesized after varying-temperature hot-dip coating (VTHDC) using large zeolite T crystals of 2 μm size and smaller T crystals of 600 nm size (see ESI Fig. S3†). The composition of the synthesis solution is 1 $SiO_2$ : 0.05 $Al_2O_3$ : 0.26 $Na_2O$ : 0.09 $K_2O$ : 35 $H_2O$ where the $H_2O/SiO_2$ is different from the previous work.[18] The crystallization reaction was kept for 4 h at 423 K. The SEM image of membrane M1 in Fig. 1c and d revealed that a continuous and dense layer composed of well intergrown rod-like crystals was formed on the support surface. The rod-like crystals formed

[a]State Key Laboratory of Fine Chemicals, School of Chemical Engineering, Dalian University of Technology, Dalian, Liaoning, 116024, China. E-mail: yjianhua@dlut.edu.cn

[b]Department of Chemical Engineering and Materials Science, University of Minnesota, Minneapolis, Minnesota 55455, USA. E-mail: tsapa001@umn.edu

[c]State Key Laboratory of Fine Chemicals, School of Petroleum and Chemical Engineering, Dalian University of Technology, Panjin, Liaoning, 124221, China

† Electronic supplementary information (ESI) available. See DOI: 10.1039/c7ta04521b

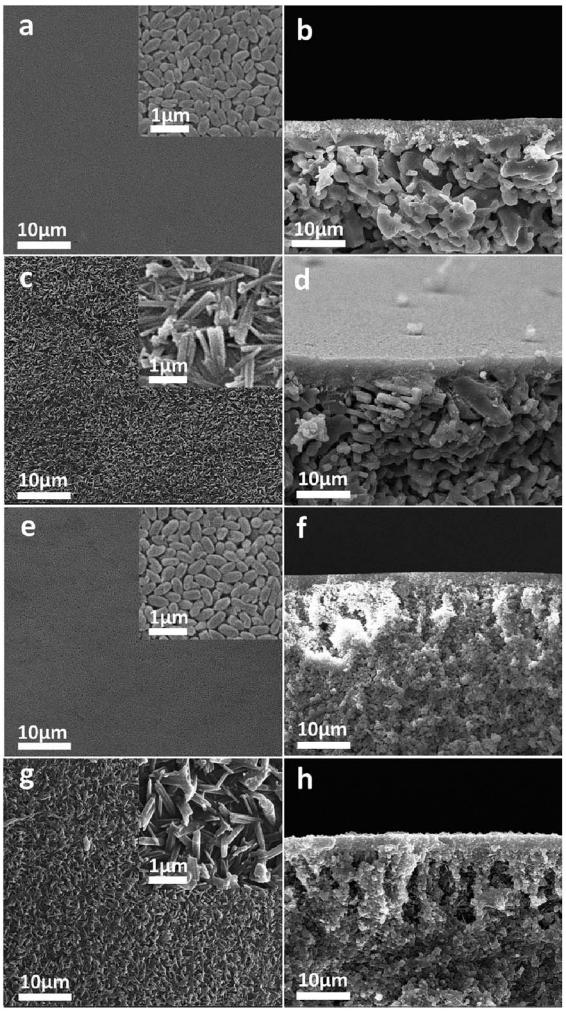


Fig. 1 SEM images of the M1 seed layer (a) & (b) and the zeolite T membrane (c) & (d) on a macroporous $Al_2O_3$ tube after varying-temperature hot-dip coating, and the M2 seed layer (e) & (f) and the zeolite T membrane (g) & (h) on a hollow fiber (HF) support after varying-pressure vacuum seeding.

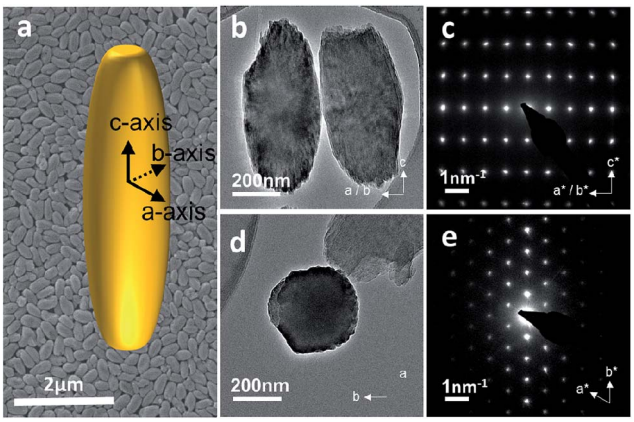


Fig. 2 (a) SEM image and schematic of zeolite T particle morphology elongated along the *c*-axis. (b) BF-TEM image of the zeolite-T particle oriented along the *a*- or *b*-crystallographic axis with its (c) corresponding diffraction pattern. (d) BF-TEM image of the particle oriented along the *c*-axis and its (e) corresponding diffraction pattern.

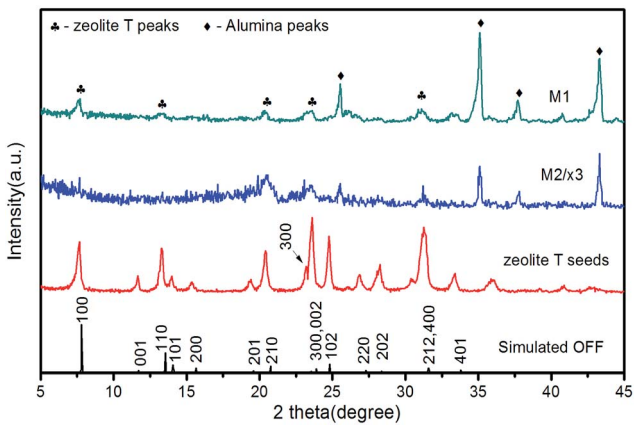


Fig. 3 XRD patterns of simulated zeolite OFF, zeolite T seeds (600 nm), M1 ($Al_2O_3$ support) and M2 (HF support, magnified 3 times) at 423 K for 4 h.

were distinct from the rice-like seeds. TEM images and electron diffraction patterns of zeolite T seed crystals in Fig. 2 reveal that the seeds are elongated along the *c*-axis while the short axis is along *a*- and *b*-directions (*a*- and *b*-axes are crystallographically identical). The membrane possessed a thickness of 3–4 μm, which was similar to that of the seed layer. This indicates that the seeds grew mostly in-plane. The XRD pattern of membrane M1 (Fig. 3) shows the characteristic peaks of zeolite T. The (001) peak is missing, while the peaks (101), (201), (102) and (202) are weaker, (002) decreased compared to (300), which indicated that the membrane was mostly oriented with its *c*-axis parallel to the $Al_2O_3$ support surface. The preferred orientation for the water molecular permeation is the *a*- or *b*-axis since the pore window size[7] along the *a*- or *b*-axis is about 0.31 nm while the effective pore opening of the 12-ring in the *c*-orientation is small (around 0.25 nm) due to the blocking by 6-ring erionite channels (Fig. S5†). The oriented membrane M1 exhibited high permeance with a water flux of 5.9 kg $m^{-2}$ $h^{-1}$ and a $H_2O$/isopropanol (IPA) separation factor larger than 10 000 for the dehydration of 90 wt% IPA aqueous solution at 348 K. The preparation of zeolite T membranes was also attempted on home-made hollow fibers (denoted as HF, see ESI Fig. S1†) with an outer diameter of 1.6 mm as well, using a similar procedure to that used for membrane M1. A well-packed and uniform T seed layer with a thickness of 3–4 μm can be formed on the surface of the HF support (see Fig. 1e and f) using varying-pressure vacuum seeding (VPVS) proposed by us. The resulting zeolite membrane M2 exhibited a similar membrane morphology to membrane M1 in Fig. 1g and h. A continuous and dense membrane consisting of well intergrown and rod-like crystals with the *c*-axis parallel to the support surface was observed. Indeed, the membrane M2 thickness of 3–4 μm was almost the same as the seed layer. The XRD patterns of membrane M2 (Fig. 3) confirm the formation of a pure phase zeolite T membrane. The intensity of the zeolite T layer for M2 is weaker than that for M1 as does the support despite the same

membrane thickness, because the intensity increases with increasing sample amount exposed to the X-ray beam.[19] Membrane M2 is highly permeable and selective to the dehydration of IPA aqueous solution with a water flux of 9.8 kg $m^{-2}$ $h^{-1}$ and a separation factor of 3870. It is worth noting that the VTHDC method[18] led to the formation of a discontinuous seed layer with part of the support surface not covered by seeds (see ESI Fig. S6†), resulting from the small coating driving force of temperature-driven pressure,[18] owing to the smaller thickness of the HF support. The discontinuous seed layer naturally led to a poor selectivity of the resulting membrane (see ESI Table S1†).

To get insights into the membrane growth process, membrane M1 was traced at various time stages of growth (Fig. 4). For membrane M1 after 1 h of growth, some small particles as marked by red circles in Fig. 3a1 emerged on the seed crystals. With increasing the crystallization time to 2 h, the seeds became larger and interconnected and the voids became small. Interestingly, the membrane thickness from 1 h to 2 h remained almost the same as the seed layer of 3–4 μm. At the time period of 2 h, considerable changes were observed on the membrane surface. The seeds became well intergrown, with one end of some rice-like seeds elongating to have an appearance of a rod-like "tail" as marked by red circles in Fig. 3c1. The membrane thickness after 2 h growth remained the same. At 3 h, the membrane surface was compactly covered by well intergrown rod-like crystals. When the time increased to 4 h, the rod-like crystals elongated further with increased intergrowth. The key element of this growth process is that the membrane thickness remained the same during an initial growth period of 3 h with minor changes in thickness observed at the end of 4 h growth.

The above time tracking observations revealed that membrane M1 was formed by an epitaxial growth of seeds with closing of the voids between the seeds as illustrated in Fig. 5. Although the nucleation process took place as well and a few new nuclei appeared on the seed layer at the early stage of 1–2 h, judged by the unchanged membrane thickness, the formed nuclei did not contribute to columnar growth and possibly were dissolved in the solution to provide nutrients for the crystal growth according to Ostwald Ripening.[20] It is very interesting that at the early stage of the growth before 2 h, the seeds became thicker along *a*- and *b*-directions, leading to the size increase of the rice-like seed grains and closing of the seed voids. After 2 h, the seeds grew along the *c*-direction, leading to the formation of rod-like crystals. According to the XRD patterns from 1 h to 3 h in Fig. S7,† the intensity of the (100) and (210) peaks increased

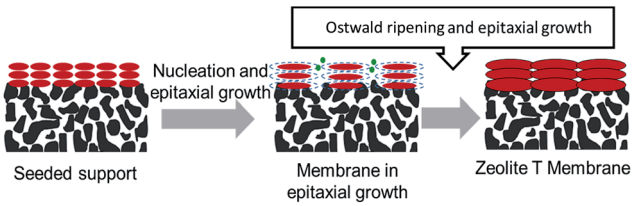


Fig. 5 Schematic of a new growth mechanism of the zeolite T membrane.

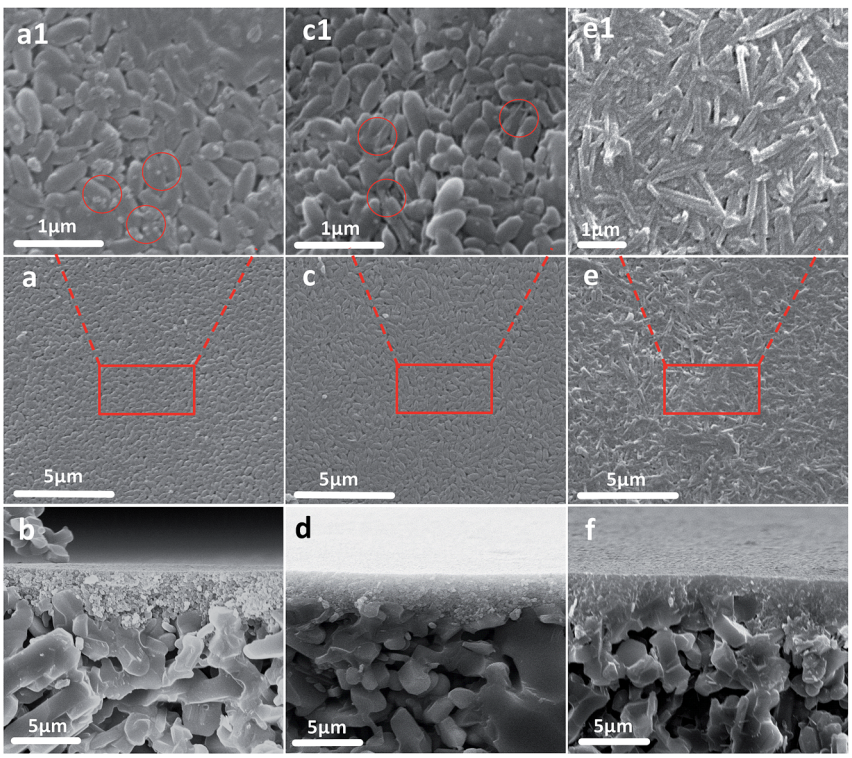


Fig. 4 SEM images of the top view and cross-section of prepared zeolite T membranes at 423 K for different crystallization times: (a1), (a) and (b) for 1 h, (c1), (c) and (d) for 2 h, and (e1), (e) and (f) for 3 h.

 

while the peaks (201) became weak as the crystallization time increased. As a result, the peak intensity I (300) increased while I (002) decreased from 1 h to 3 h, further supporting the preferential growth of a–c and b–c planes. It is worth noting that the TEM image of the sample (see ESI Fig. S8†) collected from the bottom of the autoclave for the membrane M1 growth exhibited an amorphous phase structure, indicating that no T crystals can be formed by the homogeneous growth from the solution. This provides evidence for the heterogeneous growth of seeds for the resulting zeolite T membrane.

Compared with other reported zeolite T membranes in the literature, our membranes M1 and M2 are the thinnest, resulting in high flux with high selectivity (see Table S2†). Except the membrane from fluoride media reported by Chen *et al.*,[21,22] the reported T zeolite membranes were obtained from a more concentrated synthesis gel at a lower temperature of 373 K with longer crystallization time (>30 h).[23] In these cases, it is speculated that the nucleation from the synthesis gel is dominant over the seed epitaxial growth shown in Fig. S9,† and therefore the closure of voids by slow epitaxial growth is not observed. Only after long time periods of growth of the nuclei the formation of a thick intergrown zeolite T layer is observed. In our work, the synthesis time of zeolite T membranes was largely shortened to 4 h at 423 K by the epitaxial growth through kinetic control of the crystallization. The good acid resistance was revealed by the long-time acid resistance test where the water flux decreased from 5.9 and then reached a steady-state of 4.7 kg $m^{-2}$ $h^{-1}$ in the test period, and the water permeate concentration remained above 99.8 wt% through the experiment at pH of 5 (Fig. S10†). Our membranes also showed good reproducibility through repeat experiments (Table S3†). Furthermore, the membrane was reduced to almost the same thickness as that of the seed layer and high flux with high selectivity was obtained. This will largely reduce the cost of zeolite-T membranes, thereby making them favorable for wide industrial applications.

## Conclusions

In summary, dense and continuous zeolite T membranes with the thickness almost similar to that of the seed layer could be obtained both on macroporous coarse $Al_2O_3$ tubes and on hollow fiber supports at a higher temperature of 423 K with a shorter synthesis time of 4 h. The as-synthesized membranes on $Al_2O_3$ tubes and hollow fiber supports showed a high flux of 5.9 and 9.8 kg $m^{-2}$ $h^{-1}$, respectively, with a high selectivity of >10 000 and 3870, respectively, at 348 K for a 90% isopropanol/water mixture. Tracking the membrane growth process at various synthesis times suggests that the dense zeolite T membranes in the present work are formed *via* epitaxial growth of seeds in *a*- and *b*-planes with closure of voids between the seeds at the investigated temperature of 423 K. Therefore, the zeolite T membrane thickness was restricted to 3–4 μm, with almost similar thickness to that of the seed layer. Good reproducibility and acid resistance were demonstrated for the synthesized membranes. High performance and largely shortened membrane growth time are favourable for wide industrial implementation of membrane separation because of the reduced cost. This work demonstrates that regulating the kinetics of zeolite growth is fundamental, highly effective and a simple approach to achieve low cost high-performance membranes.

## Acknowledgements

The financial support from the National Natural Science Foundation of China (No. 21376036 and 21236006), the National High Technology Research and Development Program of China (No. 2015AA03A602) and the Fundamental Research Funds for the Central Universities of China (No. DUT15ZD(G) 03) is acknowledged. TEM work was supported by the Center for Gas Separations Relevant to Clean Energy Technologies, an Energy Frontier Research Center funded by the US Department of Energy, Office of Science, Basic Energy Sciences under Award DE-SC0001015. The authors thank Prof. Zhengbao Wang for providing hollow fiber supports.

## Notes and references

1 J. Coronas and J. Santamaría, *Sep. Purif. Methods*, 1999, **28**, 127–177.
2 A. Tavolaro and E. Drioli, *Adv. Mater.*, 1999, **11**, 975–996.
3 N. Rangnekar, N. Mittal, B. Elyassi, J. Caro and M. Tsapatsis, *Chem. Soc. Rev.*, 2015, **44**, 7128–7154.
4 Y. Morigami, M. Kondo, J. Abe, H. Kita and K. Okamoto, *Sep. Purif. Technol.*, 2001, **25**, 251–260.
5 J. Caro, M. Noack and P. Kölsch, *Adsorption*, 2005, **11**, 215–227.
6 Y. Hasegawa, T. Nagase, Y. Kiyozumi, T. Hanaoka and F. Mizukami, *J. Membr. Sci.*, 2010, **349**, 189–194.
7 R. L. Gorring, *J. Catal.*, 1973, **31**, 13–26.
8 Y. Cui, H. Kita and K. I. Okamoto, *J. Membr. Sci.*, 2004, **236**, 17–27.
9 H. Zhou, Y. Li, G. Zhu, J. Liu and W. Yang, *Sep. Purif. Technol.*, 2009, **65**, 164–172.
10 Z. Lai, M. Tsapatsis and J. P. Nicolich, *Adv. Funct. Mater.*, 2004, **14**, 716–729.
11 R. Zhou, L. Hu, Y. Zhang, N. Hu, X. Chen, X. Lin and H. Kita, *Microporous Mesoporous Mater.*, 2013, **174**, 81–89.
12 J. Yang, L. Li, W. Li, J. Wang, Z. Chen, D. Yin, J. Lu, Y. Zhang and H. Guo, *Chem. Commun.*, 2014, **50**, 14654–14657.
13 J. Choi, H. Jeong, M. A. Snyder, J. A. Stoeger, R. Masel and M. Tsapatsis, *Science*, 2009, **325**, 590–593.
14 J. Yao, D. Dong, D. Li, L. He, G. Xu and H. Wang, *Chem. Commun.*, 2011, **47**, 2559–2561.
15 J. Hedlund, M. Noack, P. Kolsch, D. Creaser, J. Caro and J. Sterte, *J. Membr. Sci.*, 1999, **159**, 263–273.
16 K. Varoon, X. Zhang, B. Elyassi, D. D. Brewer, M. Gettel, S. Kumar, J. A. Lee, S. Maheshwari, A. Mittal, C. Y. Sung, M. Cococcioni, L. F. Francis, A. V. McCormick, K. A. Mkhoyan and M. Tsapatsis, *Science*, 2011, **334**, 72–75.

17 W. C. Yoo, J. A. Stoeger, P. S. Lee, M. Tsapatsis and A. Stein, *Angew. Chem., Int. Ed.*, 2010, **49**, 8699–8703.
18 X. Chen, J. Wang, D. Yin, J. Yang, J. Lu, Y. Zhang and Z. Chen, *AIChE J.*, 2013, **59**, 936–947.
19 F. H. Chung, *J. Appl. Crystallogr.*, 1974, **7**, 526–531.
20 N. J. J. Johnson, A. Korinek, C. Dong and F. C. J. M. Van Veggel, *J. Am. Chem. Soc.*, 2012, **134**, 111068–111071.
21 R. F. Zhou, F. Zhang, N. Hu, X. S. Chen and H. Kita, *Chem. Lett.*, 2011, **40**, 1383–1385.
22 F. Zhang, Y. Zheng, L. Hu, N. Hu, M. Zhu, R. Zhou, X. Chen and H. Kita, *J. Membr. Sci.*, 2014, **456**, 107–116.
23 X. Wang, Y. Chen, C. Zhang, X. Gu and N. Xu, *J. Membr. Sci.*, 2014, **455**, 294–304.